Photophysicochemical and photodynamic therapy properties of metallophthalocyanines linked to gold speckled silica nanoparticles

Edith Dube[a], David O. Oluwole[a], Nwaji Njemuwa[a], Earl Prinsloo[b], Tebello Nyokong[a],*

[a] Center for Nanotechnology Innovation, Department of Chemistry, South Africa
[b] Biotechnology Innovation Centre, Rhodes University, Grahamstown 6140, South Africa

A B S T R A C T

This work reports on the linkage of 2(3),9(10),16(17),23(24) tetrakis [(benzo[d]thiazol-2-yl phenoxy) phthalocyaninato] zinc(II) (1) and indium(III) chloride (2) to gold speckled silica (GSS) nanoparticles via gold to sulphur (Au-S) and gold to nitrogen (Au-N) self-assembly to form the conjugates: 1-GSS and 2-GSS. The formed conjugates were characterized using microscopic and spectroscopic techniques, and the photophysicochemical properties and photodynamic therapy (PDT) activity against human breast adenocarcinoma cell line (MCF-7 cells) were studied. The conjugates afforded decrease in fluorescence quantum yields with corresponding increase in triplet and singlet oxygen quantum yields when compared to phthalocyanines alone. Singlet oxygen is cytotoxic to cancer cells hence it is important for PDT. The in vitro dark toxicity of complex 2 and 2-GSS against MCF–7 cells showed ≥ 93% viable cells within concentration ranges of 10–160 μg/mL. 2–GSS showed enhanced PDT activity with less than 50% viable cells at 80 μg/mL as compared to 2 and GSS alone which showed > 60% viable cells within 10–160 μg/mL. The observed improvements in the PDT activity of 2-GSS could be attributed to the high singlet oxygen generation of 2-GSS compared to 2 alone in addition to the phototoxicity of GSS.

1. Introduction

Phthalocyanines (Pcs) are aromatic macrocyclic compounds composed of four isoindole units linked by nitrogen atoms [1,2]. The macrocycle can accommodate most metal ions in the central cavity, hence a range of different metal/metalloid phthalocyanines (MPcs) have been synthesized [1,3]. Depending on the central metal, MPcs are characterised by high triplet state and singlet oxygen quantum yields, and long triplet lifetimes, making them ideal candidates as photosensitizers (PS) for photodynamic therapy (PDT) [4–6]. Pcs with diamagnetic metals such as Zn^{2+}, Al^{3+}, Ga^{3+} and In^{3+} have shown great potential as PDT agents [4,7–9].

Pcs are capable of absorbing visible light, which excites them to an excited singlet state, consequently populating the excited triplet state through the intersystem crossing. Subsequently the excited triplet state transfers its energy to the ground state molecular oxygen generating a reactive oxygen species that destroys tumour cells [10]. The presence of heavy atoms in the central cavity of these Pcs gives rise to improved triplet quantum yields through spin orbit coupling (also known as heavy atom effect) which promotes intersystem crossing of the PS from the singlet excited state to the triplet state [11–13]. High triplet and singlet oxygen quantum yields are important for PDT as explained

before. However, poor selectivity of MPcs towards cancer cells is still a major challenge in the application of these PSs for PDT hence they are now linked to nanocarriers for improved targeting through enhanced permeability and retention (EPR) effect [14–16].

Nanoparticles have shown potential as drug carriers for the intracellular delivery of therapeutics [14]. Gold and silica nanoparticles have attracted attention in biomedical applications, due to their excellent biocompatibility, and ease of surface modification [17–20]. The presence of gold in the nanocarrier is expected to improve the triplet quantum yield through the heavy atom effect of gold. Additionally, gold nanoparticles upon irradiation generate heat and have been used for photothermal therapy (PTT) [21,22]. The combination of silica and gold in gold speckled silica (GSS) nanoparticles has demonstrated high thermal stability and good PTT activity in vitro using the lung cancer cell line (A549) [23]. The localized rise in the temperature of GSS particles is thought to lead to the rapid injury and death of the cells [23,24]. Hence the combination of GSS with Pcs is expected to improve the singlet oxygen generation and PDT activity of Pcs.

In this work, we report on the linkage of GSS nanoparticles to 2(3),9(10),16(17),23(24) tetrakis[(benzo[d]thiazol-2-yl phenoxy) phthalocyaninato] zinc(II) (complex 1) and 2(3),9(10),16(17),23(24) tetrakis [(benzo[d]thiazol-2-yl phenoxy) phthalocyaninato] indium(III)

---

* Corresponding author.
  E-mail address: t.nyokong@ru.ac.za (T. Nyokong).

chloride (complex **2**), using gold to sulphur (Au-S) or gold to nitrogen (Au-N) self-assembly. We have reported on the linkage of thiophineethoxy functionalized MPcs to GSS before [25], however linkage of GSS to benzothiazole substituted complexes **1** and **2**, together with the PDT activity of Pc-GSS conjugates are reported here for the first time.

The anticancer activity [26] and photosensitizing ability [27] of benzothiazole derivatives has been reported, hence incorporation of the benzothiazole moiety in this work is expected to improve the photosensitizing property and PDT activity. The formed conjugates were characterized and the photophysicochemical properties and PDT activity against human breast adenocarcinoma cell line (MCF-7 cells) were studied using complex **2** and **2**-GSS. Complex **2** and **2**-GSS were chosen for PDT studies as examples since they displayed higher triplet and singlet oxygen quantum yields compared to complex **1** and **1**-GSS respectively.

2. Experimental

2.1. Materials

N,N-Dimethyl formamide (DMF) and dimethyl sulfoxide (DMSO) were purchased from Merck. Unsubstituted zinc phthalocyanine (ZnPc), 1,3-diphenylisobenzofuran (DPBF) and anthracene-9,10-bis-methylmalonate (ADMA) were obtained from Sigma–Aldrich. Absolute ethanol was obtained from SAARCHEM. All other reagents and solvents were sourced from commercial suppliers and used as received. Ultra-pure water was obtained from a Milli–Q Water System (Millipore Corp, Bedford, MA, USA). AlPcSmix (mixture of sulfonated phthalocyanine derivatives) was used as a standard for singlet oxygen quantum yields in aqueous media and was synthesized according to literature methods [28]. The syntheses of 2(3),9(10),16(17),23(24) tetrakis[(benzo[*d*]thiazol-2-yl phenoxy) phthalocyaninato] zinc(II) (**1**) [27], 2(3),9(10),16(17),23(24) tetrakis[(benzo[*d*]thiazol-2-yl phenoxy) phthalocyaninato] indium(III) chloride (**2**) [29] and (3-aminopropyl) triethoxysilane (APTES) functionalized gold speckled silica (GSS) nanoparticles [25], have previously been reported in the literature.

For PDT studies, cultures of human breast adenocarcinoma cells (MCF-7) were acquired from Cellonex. Dulbecco's phosphate-buffered saline (DPBS), Dulbecco's modified Eagle's medium (DMEM), trypan blue and trypsin were acquired from Sigma Aldrich®. 100 µg/mL-penicillin-100 unit/mL-streptomycin-amphotericin B mixture, heat-inactivated fetal calf serum (FCS) and cell proliferation neutral red reagent (WST1) were acquired from Roche®.

Equipment employed is presented in supporting information

2.2. Linkage of complexes 1 and 2 to GSS (Scheme 1)

The synthesis of complexes **1, 2** and **GSS** has been previously reported [25,27,29]. For the synthesis of the phthalocyanine–GSS conjugates: complex **1** (0.02 g, 0.013 mmol) or complex **2** (0.02 g, 0.009 mmol) were dissolved in dry DMF (2 mL) and GSS (0.05 g in 3 mL ethanol) was added and the reaction mixture was stirred for 24 h at room temperature. The conjugates were centrifuged, successively washed with ethanol and allowed to dry in the fume hood. The conjugates are represented as **1**-GSS and **2**-GSS.

3. Results and discussion

3.1. Characterization of the conjugates

Scheme 1 shows the linking of the Pcs (complexes **1** and **2**) to GSS nanoparticles through either Au-S or Au-N self-assembly since the complexes have both sulphur and nitrogen in their substituents.

3.1.1. Electronic absorption spectra of complexes and their conjugates

The normalized absorption spectra of complexes **1** and **2** in DMSO

(Fig. 1A) show narrow, single intense Q bands at 681 and 690 nm respectively (Table 1), typical of the monomeric behaviour of metalated phthalocyanines with degenerate D_{4h} symmetry [30]. Due to the non-planar effect of the indium(III) ion, with a relatively bigger atomic radius than the zinc(II) as the central metal ion in the Pc cavity [31,32], the Q band of complex **2** is red shifted as compared to complex **1**, Fig. 1A, Table 1. GSS alone shows intense absorption between the Q band and 500 nm (Fig. 1**B(a)**), attributed to the presence of nanogold. Pc complexes alone show minimum to no absorption between 470 nm and 560 nm (Fig. 1A), however an enhancement in absorption was observed (Fig. 1**B(b,c)**) after conjugation of the complexes to GSS, which could be attributed to the presence of GSS in the conjugate since GSS absorbs within this region (Fig. 1**B(a)**).

Complexes **1**, **2** and their conjugates with GSS are not soluble in water, hence for studies in water, they were first dissolved in 50 µL DMSO and then diluted with water to 5 mL (1% (v/v) DMSO). Aqueous media is important for biological applications. In aqueous media (Fig. S1, ESI†), broad Q bands were observed signaling extensive aggregation. Aggregation in Pcs results from π–π stacking interaction of the aromatic rings of Pcs [33]. The effect of aggregation is usually reduced by solubilization of the drug in a biocompatible surfactant for therapeutic formulations.

The loading of complexes **1** and **2** onto the nanoparticles was investigated following literature methods [34]. This involves comparing the Q band absorbance intensity of the Pc in the conjugate with that of the initial Pc before the conjugation. The values are listed on Table 1 and the amounts are about the same for the two conjugates.

An overlay of the absorption, excitation and emission spectra in DMSO are shown in Fig. 2 (using **1**-GSS, as an example). The absorption spectrum is broader than the excitation spectrum. The excitation spectrum is a mirror image of the emission spectrum. The closeness of the Q-band absorption and excitation maxima shows that the nuclear configurations of the ground and excited states are similar and are not affected by excitation in DMSO. It also shows that there was no aggregation in DMSO.

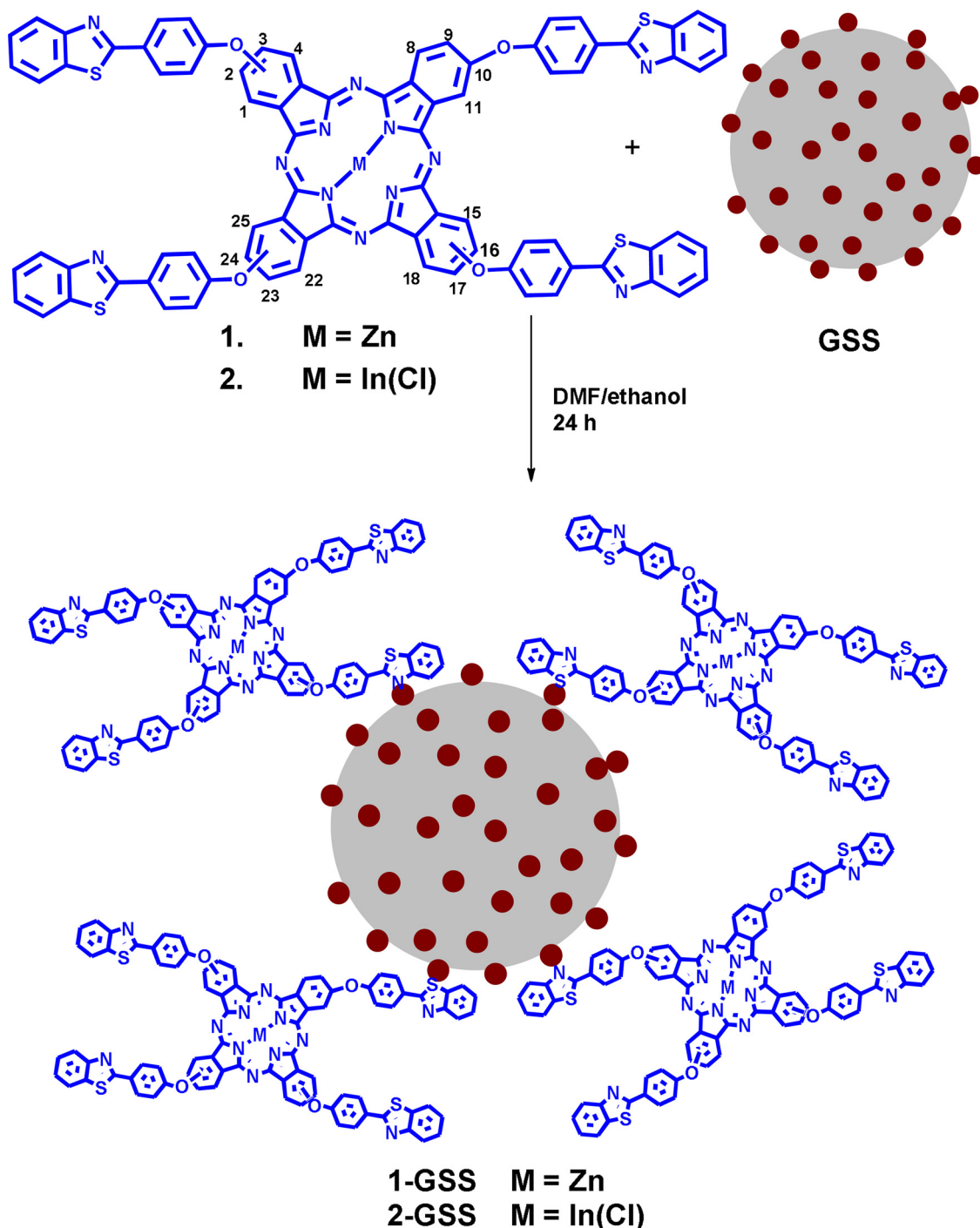### 3.1.2. Size and morphology determinations

Fig. 3 shows the TEM micrographs of the GSS and the conjugates. The zoomed insert of the GSS micrograph, Fig. 3, shows discontinuous gold nanodomains speckled across the silica surface (small darker spheres on a larger grey sphere), confirming the formation of gold speckled SiNPs (GSS). The average size of the NPs was estimated to 78.5 nm for GSS, 82.2 nm for **1**-GSS and 81.4 nm for **2**-GSS. The GSS nanoparticles alone are aggregated and aggregation intensified after linkage to the Pcs especially for **2**-GSS. Increased aggregation upon conjugation is usually due to π-π stacking between Pcs on adjacent NPs. Pcs are known for their tendency to π-π stack forming H aggregates [33] as stated above.

The powder XRD patterns for GSS, **2**-GSS and complex **2**, are shown in Fig. 4, as examples. Complex **2** exhibited broad peaks between $2\theta = 10°$ to $35°$, typical of phthalocyanines, depicting their amorphous nature [35]. GSS exhibited sharp peaks at $2\theta = 37.5°$, $44.3°$, $64.3°$, $76.9°$ and $80.8°$ (matching the pattern in card number, 03-065-2870; NIST:N AL3280 from the powder diffraction database), indicating crystallinity, attributed to the presence of gold [36], however slight broadness was observed between $2\theta = 10°$ to $30°$ probably due to the presence of silica. The conjugate **2**-GSS exhibited a similar diffraction pattern as GSS, with increase in the intensity of the peak between $2\theta = 10°$ to $30°$ due to the presence of complex **2** as explained before.

Size estimates from XRD were obtained only for the gold nanoparticles on silica before and after conjugation using the Debye–Scherrer [37] Eq. (1), by focusing on the (111) peaks (Fig. 4):

$$d = \frac{k\lambda}{\beta \cos\theta}$$

(1)

where λ is the wavelength of the X-ray source (1.5405 Å), k is an

Scheme 1. Synthetic pathways for **1**-GSS and **2**-GSS.

empirical constant equal to 0.9, β is the full width at half maximum of the diffraction peak and θ is the angular position. The sizes of the AuNPs part of the GSS were 4.54 nm, 6.01 nm and 6.27 nm for GSS, **1**-GSS and **2**-GSS, respectively (Table 1). The increase in size of the AuNPs part of GSS on conjugation may be attributed to aggregation as discussed above.

Dynamic light scattering (DLS) was used to determine the size of GSS and its conjugates in solution. As shown in Fig. 5, the size of GSS nanoparticles was 81.7 nm and upon conjugation, the size increased to 88.1 nm and 86.4 nm for **1**-GSS and **2**-GSS, respectively, Table 1, showing that the complexes were successfully adsorbed on the surfaces of the GSS. The sizes are slightly higher than obtained in TEM mainly because in TEM, the particles are in a dry state, while in DLS they are in solution.

3.1.3. FT-IR

FT-IR spectroscopy (**Fig. S2**, ESI†) was employed to assess the functional groups present on GSS and the conjugates. GSS exhibited a distinct band at 1063 cm^{-1} corresponding to the siloxane band (Si-O-Si) from silica. The spectra of the conjugates looked similar to that of GSS with the intense siloxane bands dominating the spectra making it difficult to see other bands. Consequently, FTIR cannot be conclusively used to confirm the conjugation of the complexes to the gold speckled silica nanoparticles, hence XPS will be used to confirm the linkage.
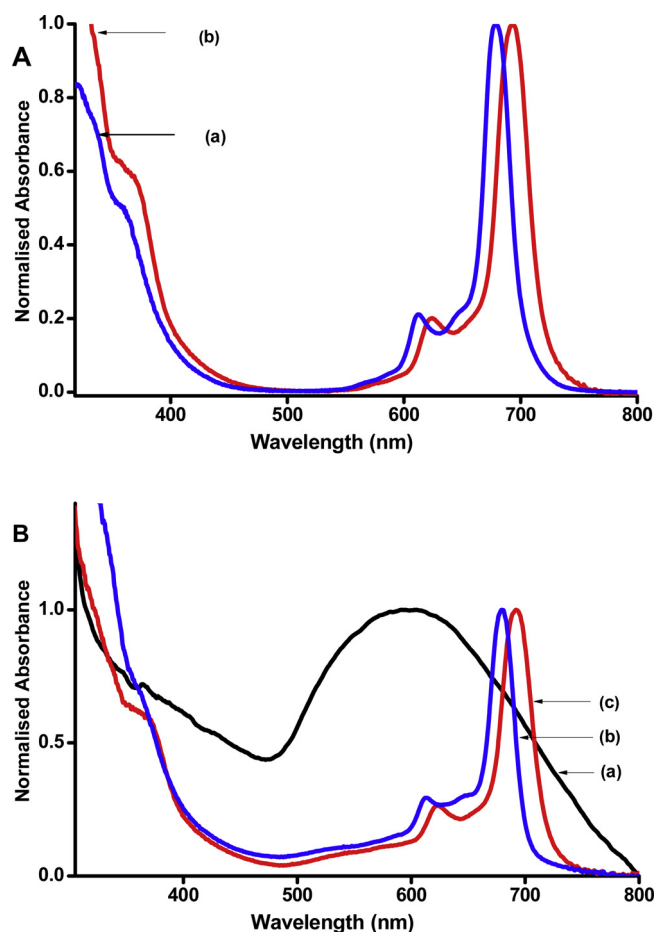
Fig. 1. UV–vis absorption of (A) complex **1** (a) and complex **2** (b) in DMSO and (B) GSS (a), **1**-GSS (b) and **2**-GSS (c) in DMSO.

Fig. 2. Emission (a), excitation (b) and absorption (c) spectra of **1**-GSS (excitation = 609 nm, solvent = DMSO).

3.1.4. XPS Spectra

XPS analysis was used to confirm interaction between GSS and the complexes. Fig. 6A shows the XPS survey spectra and the respective binding energies for GSS, complex **2** and **2**-GSS as representatives. GSS showed the presence of Si (2.6 eV and 101.3 eV), Au (83.8 eV, 334.9 eV and 351.7 eV), C (281.2 eV), N (396.4 eV) and O (531.5 eV). C, N and O are from APTES used for the functionalisation of silica. Complex **2** exhibited S (161.7 eV), C (281.5 eV), N (396.3 eV), O (532.1 eV), In (445.4 eV) and Cl (227.83 eV), while the conjugate **2**–GSS displayed similar elements as complex **2**, but with additional elements, Au (83.5 eV, 332.9 eV and 352.5 eV) and Si (102.8 eV) from GSS.

The high resolution XPS analysis was employed to show the linkage of GSS to the Pc complexes, using complex **2** as an example. The S2p peak for complex **2** alone (Fig. 6B) showed two subpeaks at 161.7 eV and 162.8 eV attributed to S-C and S, respectively, while the conjugate (Fig. 6C, **2**-GSS as an example) displayed three peaks at 161.3 eV, 162.4 eV and 165.8 eV corresponding to S-C, S and S-Au, respectively.

Since the complexes contain both S and N, a nitrogen to gold interaction (N-Au) was also investigated. The N 1 s peak for complex **2** alone (Fig. S3A, ESI†) showed two subpeaks corresponding to –N–C– (396.1 eV) and –N– (397.3 eV), while the conjugates (Fig. S3B ESI†, **2**–GSS as an example) displayed three peaks attributed to –N–C– (396.0 eV), –N– (397.2 eV) and –N–Au– (399.1 eV). The presence of both gold to sulfur and gold to nitrogen interactions (–N–Au– and –S–Au–) indicates that the complexes are successfully linked to GSS through gold to sulfur and gold to nitrogen interactions. N-Au interaction is most likely from the N on the ring substituent rather than the N atoms on the phthalynine core, considering the positions of nitrogens on the macrocycle.

3.2. Photophysicochemical parameters

Table 1 shows the fluorescence quantum yields (Φ_F) and lifetimes (τ_F), triplet quantum yields (Φ_T) and lifetimes (τ_T), as well as singlet oxygen quantum yields (Φ_Δ) for **1** and **2** before and after conjugation in DMSO. The singlet oxygen quantum yields (Φ_Δ) were also determined in water (containing 1% DMSO in water).

3.2.1. Fluorescence quantum yields (Φ_F) and lifetimes (τ_F)

The Φ_F values for **1**-GSS and **2**-GSS were lower than those of the respective Pc complexes alone, indicating that the presence of GSS nanoparticles quenched the fluorescence behaviour of the complexes. This phenomenon could be attributed to the heavy atom effect resulting from gold in the GSS known to deactivate the excited singlet state thereby fostering the rapid population of the excited triplet state *via* intersystem crossing [11–13]. By the same principle, **2**-GSS containing a heavier atom indium in its central cavity displayed much lower Φ_F value as compared to **1**-GSS containing Zn. The same applies to Pcs alone.

As expected, the conjugates afforded short fluorescence lifetimes corresponding to their low fluorescence quantum yields since there is a

Table 1
Photophysicochemical parameters of complexes 1, 2 and their conjugates in DMSO.

Samples	DLS Size (nm)[a]	λ_{abs}(nm)[b]	Pc loading (µg/mg)	Φ_F (± 0.01)	$\tau_{F(ns) (\%)}$ (± 0.03)	Mean τ_F(ns)	Φ_T (± 0.02)	τ_T(µs) (± 2)	Φ_Δ[b] (± 0.01)
1[c]	–	681 (688)		0.24	2.86 (100)	2.86	0.56	130	0.50 (0.07)
1-GSS	88.1 (6.01)	680 (687)	50	0.13	2.81 (97.6) 0.18 (2.4)	2.79	0.68	132	0.59 (0.11)
2[c]	–	690 (705)		0.03	0.78 (100)	0.78	0.75	55	0.64 (0.12)
2-GSS	86.4 (6.27)	693 (701)	48	0.01	0.73 (82.1) 0.40 (17.9)	0.67	0.82	48	0.72 (0.16)

[a] numbers in brackets are for Au speckles only from XRD. The DLS particle size for GSS alone is 81.7 nm and for Au speckles alone in GSS is 4.54 nm (from XRD).
[b] numbers in brackets are the values in water (with 1% DMSO).
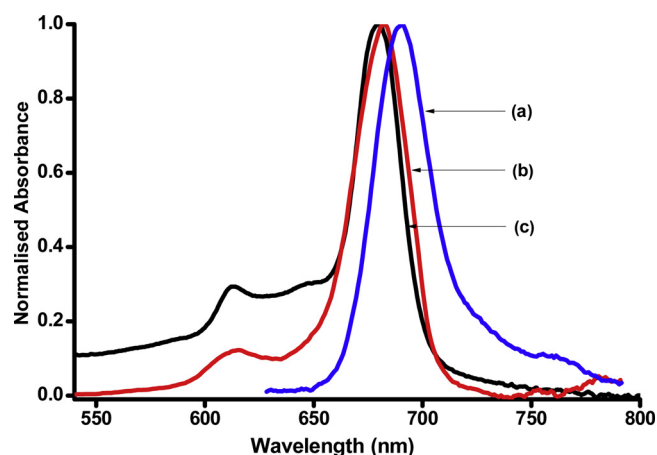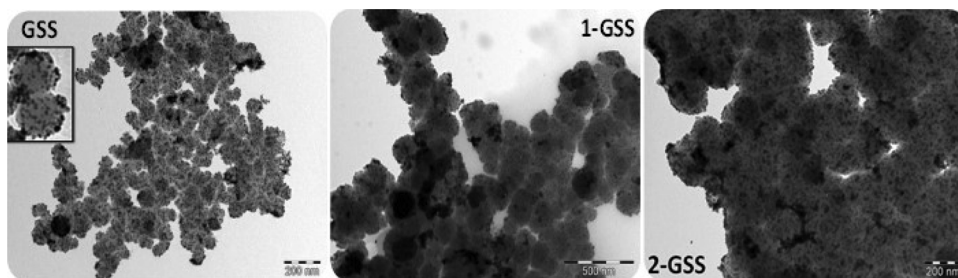[c] values in DMSO from [27].

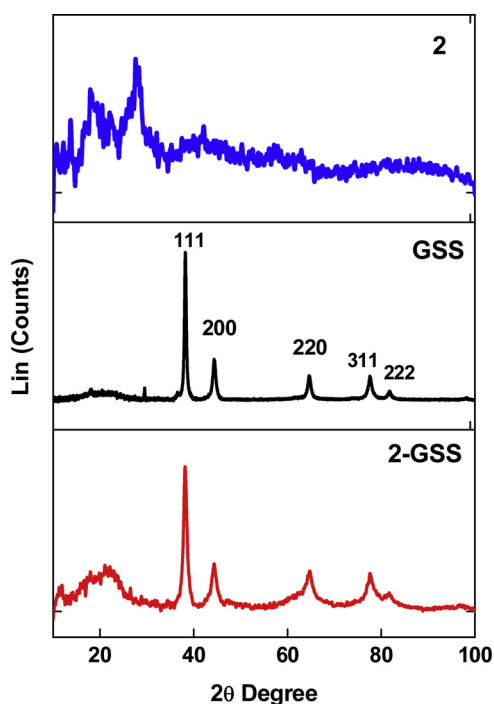**Fig. 3.** Representative TEM micrographs for GSS, **1**-GSS and **2**-GSS.

Fig. 4. XRD diffractograms for GSS, **2**-GSS, and complex **2**.

direct relationship between the former and the latter. Pcs alone showed mono-exponential decay behavior typical of monomeric derivatives [38], however the conjugates displayed a biexponential decay (Fig. 7, using **2-GSS** as example), due to the existence of two lifetimes as shown in Table 1. The biexponential lifetimes observed for the conjugates, could be associated with the monomeric non-interacting MPc molecules, while the second (shorter lifetime) is attributed to the interaction between the MPc framework on adjacent nanoparticles, resulting in unquenched and quenched photo-excited singlet states, respectively [39].
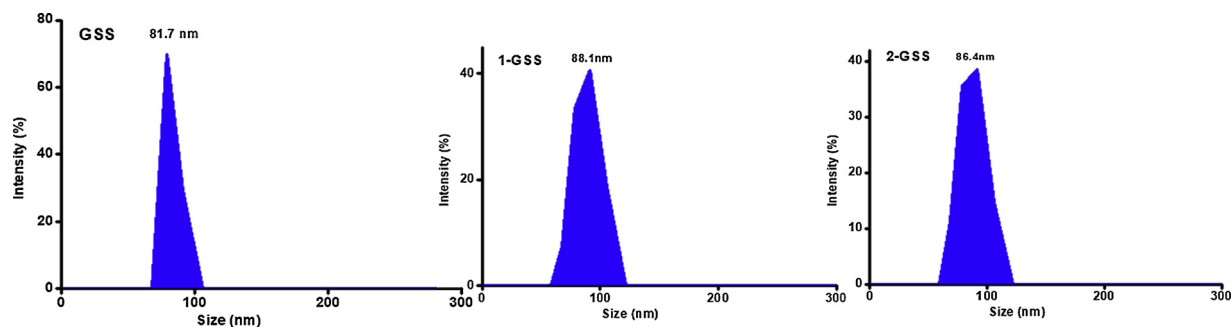
3.2.2. Triplet quantum yields (Φ_T) and lifetimes (τ_T)

The efficiency of a phthalocyanine as a photosensitizer is determined by its triplet state quantum yield (Φ_T) and lifetime (τ_T) with its corresponding low fluorescence quantum yield. A high triplet quantum yield is of great importance since it influences the singlet oxygen production.

The transient differential spectrum of **2**-GSS as an example is shown in Fig. 8**A**. This spectrum is useful in determining the excited-state dynamics of Pcs. The typical broad band between 400–600 nm with a peak centred at 495 nm, is attributed to the triplet-triplet state excited absorption ($T_1 \rightarrow T_n$). The negative peaks, attributed to the depletion or bleaching of the phthalocyanine ground state were also observed at 364 nm and at 688 nm [40].

The triplet decay curve, Fig. 8B, obeyed second order kinetics, typical of MPc complexes at high concentration (~ 10^{-5} M), due to triplet–triplet recombination [41]. Fitting the decay curve at the absorption maximum produced the triplet lifetimes and the obtained values together with the triplet quantum yields are summarized in Table 1.

The Pc complexes displayed high triplet quantum yields ($\Phi_T = 0.56$ for **1** and 0.75 for **2**), due to the presence of heavy atoms, Zn and In, as previously explained. The heavy atom effect was also confirmed by larger values of the indium complex and its conjugate compared to the zinc counterparts since indium is a heavier atom than zinc (Table 1). The heavy atom effect of gold, was likewise shown by the enhanced Φ_T on linkage of complexes to GSS. The triplet lifetimes became shorter as the triplet quantum yields increased as expected [42] except for **1**-GSS with longer lifetimes probably due to the protection of the Pc complexes by the NPs, since NPs are larger than Pcs ~1 nm. The triplet quantum yield of the complexes and their conjugates in aqueous media could not be obtained due to the aggregation tendencies of Pcs.

3.2.3. Singlet oxygen quantum yields

Singlet oxygen ($^1O_2$), is the major cytotoxic species responsible for cancer cell death in PDT [43]. The singlet oxygen quantum yield (Φ_Δ) is a measure of the ability of a photosensitizer to produce singlet oxygen. The efficiency of singlet oxygen generation of PS, mostly depends on the energy transfer from the triplet state to ground state molecular oxygen [44]. To determine the singlet oxygen quantum yield, the chemical photodegradation of singlet oxygen quenchers (DPBF in
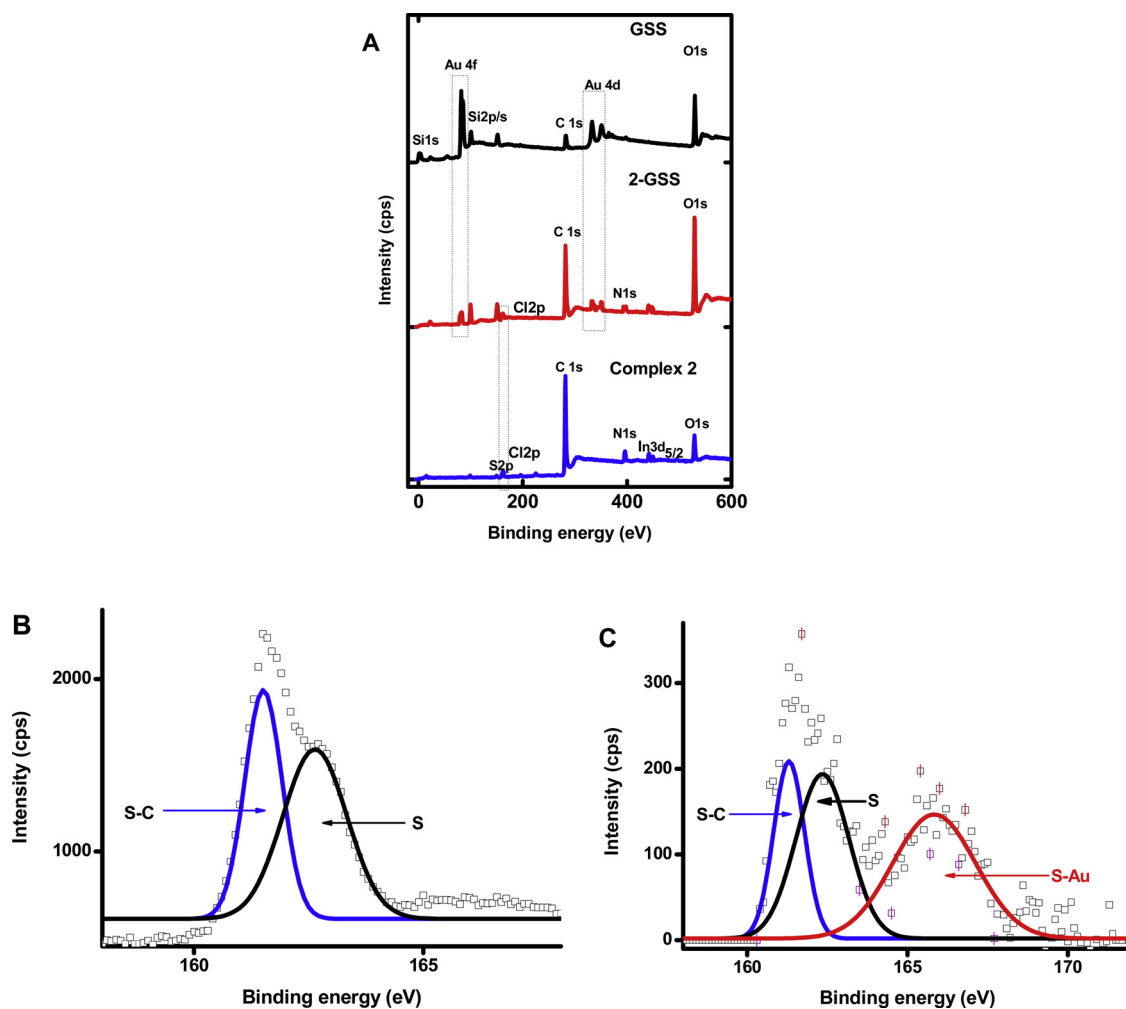

Fig. 5. Dynamic light scattering curves for GSS, **1**-GSS, and **2**-GSS.

Fig. 6. XPS spectra (A) survey spectra for GSS, complex **2** and **2**-GSS, (B) and (C) high resolution S2p spectra for **2** and **2**-GSS, respectively.
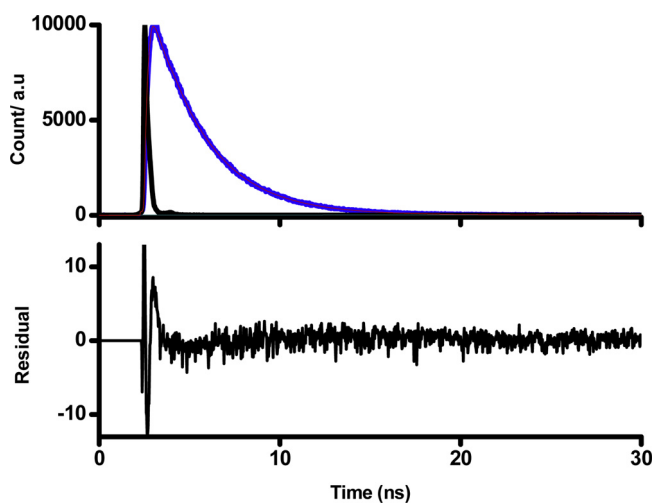

Fig. 7. Fluorescence decay (blue), χ^2 fitting (red) and IRF (black) curves for complex **2**-GSS in DMSO.

DMSO, using **1**-GSS as an example and ADMA in aqueous media (1% DMSO), using complex **2** as an example) was monitored over a period of time (Fig. 9). The Q-bands of the complexes and their conjugates remained unchanged while the singlet oxygen quenchers degraded, proving the photo-stability of Pc complexes and their conjugates over the irradiation period. Since the Φ_Δ value is dependent on the Φ_T

parameter, similar trend as the latter was observed, however values in water are low (Φ_Δ = 0.07, 0.11, 0.12, 0.16 for **1**, **1**-GSS, **2** and **2**-GSS respectively) due to aggregation. Aggregation reduces the excited state lifetimes and the photosensitizing efficiency, probably due to enhanced radiationless excited state dissipation which therefore lowers the quantum yields of the excited states and of singlet oxygen generation. This could also be due to the quenching effect of water on the singlet oxygen generation of the PS due to the presence of O−H vibration in water which has been reported to negatively influence the singlet oxygen generation of the PS [45]. Additionally, it can be due to the absorption of water at around 1270 nm which is where singlet oxygen's emission wavelength is observed [45]. However, it should be noted that PS such as lutetium texaphyrin with low Φ_Δ values in water (0.11) have been employed for clinical application in PDT [46], hence these conjugates can still be applicable in PDT.

3.3. Cell studies

The *in vitro* dark cytotoxicity and photodynamic therapy (PDT) studies were carried out as reported in the literature [47].

The *in vitro* dark cytotoxicity and the photodynamic therapy studies of the PS (**2** and **2**–GSS) were tested against MCF-7 cells. Complex **2** and its conjugate were chosen for PDT studies since they displayed the highest Φ_T and Φ_Δ. Cell studies of the PS were carried out using 1% DMSO in culture media representing highest concentration of DMSO in supplemented media used for PS gradient concentration range. The vehicle control *i.e.* 1% DMSO in culture media (Fig. 10) and static
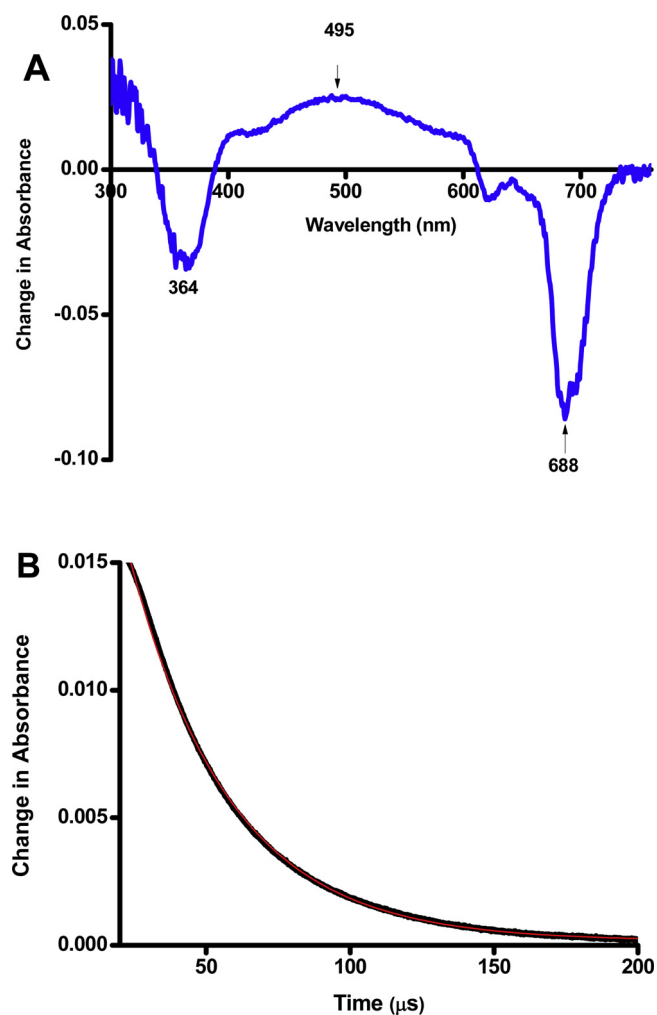
Fig. 8. (A) Transient curve and (B) Triplet absorption decay curve (black) and fitting (red) for **2**-GSS in DMSO.

Fig. 9. Spectra for singlet oxygen quantum yield determination using a photochemical method. The spectra show the degradation of (A) DPBF (initial concenrtration 3.1×10^{-5}M) in the presence of **1**–GSS (5.8×10^{-6}M) in DMSO (insert shows a plot of ΔA of DPBF at 417 nm *vs.* irradiation time) and (B) ADMA (initial concentration 1.7×10^{-5}M) in the presence of complex **2** (2.1×10^{-6}M) in water (insert shows a plot of ΔA of ADMA at 380 nm *vs.* irradiation time).

control *i.e.* culture media alone, were tested against MCF-7 cells, and their percentage cell viability were proportionately the same showing that the 1% DMSO in culture media is innocuous against the cells. Gradient PS concentration range of 10 μg/mL–160 μg/mL for *in vitro* dark cytotoxicity and PDT were used.

3.3.1. In vitro dark cytotoxicity

Complex **2**, GSS and **2**-GSS (Fig. 10), exhibited ≥ 93% viable cells at concentration ≤160 μg/mL showing that complex **2** and its conjugate are relatively innocuous towards the MCF-7 cells in the absence of light which is a good indication for an ideal photosensitizer for PDT. Dark cytotoxicity is undesirable in PDT applications as it results in cytocidal activity against both healthy and tumour cells. The absence of dark toxicity makes complex **2** and **2**-GSS good candidates for PDT. GSS alone also showed no toxicity in the absence of light.

3.3.2. Photodynamic therapy activity

The PDT activity of the samples was achieved under the same conditions as the dark cytotoxicity study but with a fixed light dosimetry of 170 J/cm^2. When MCF-7 cancer cells were treated with the highest concentration of complex **2** (160 μg/mL), 66% of the cells were still viable (Fig. 10A), even though the Φ_Δ in DMSO was high (0.64). The high percentage cell viability in the presence of **2** could be attributed to aggregation of the complex in aqueous media as also shown by the low Φ_Δ (0.12) values in water. However, it should be noted that the photo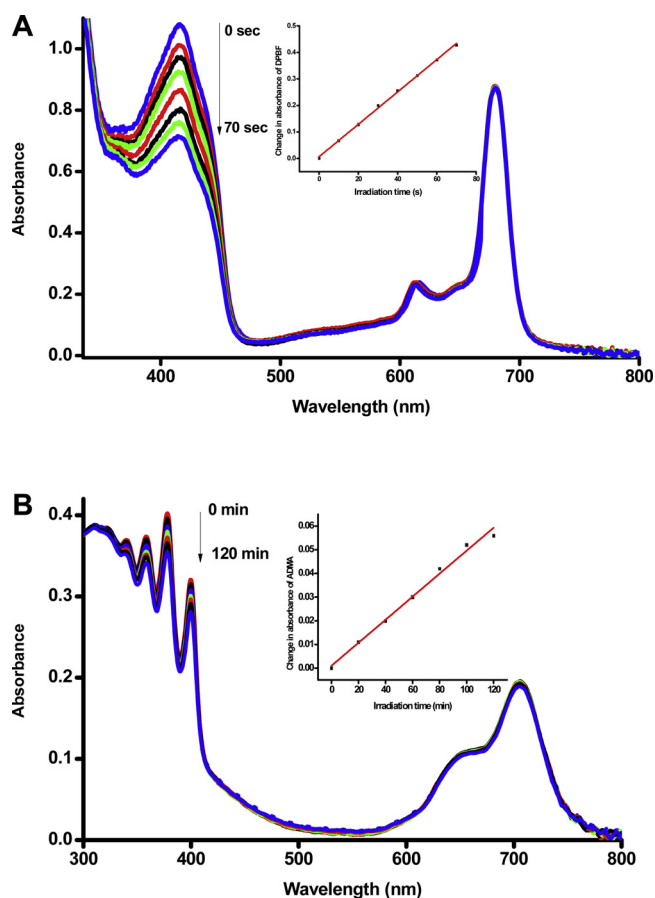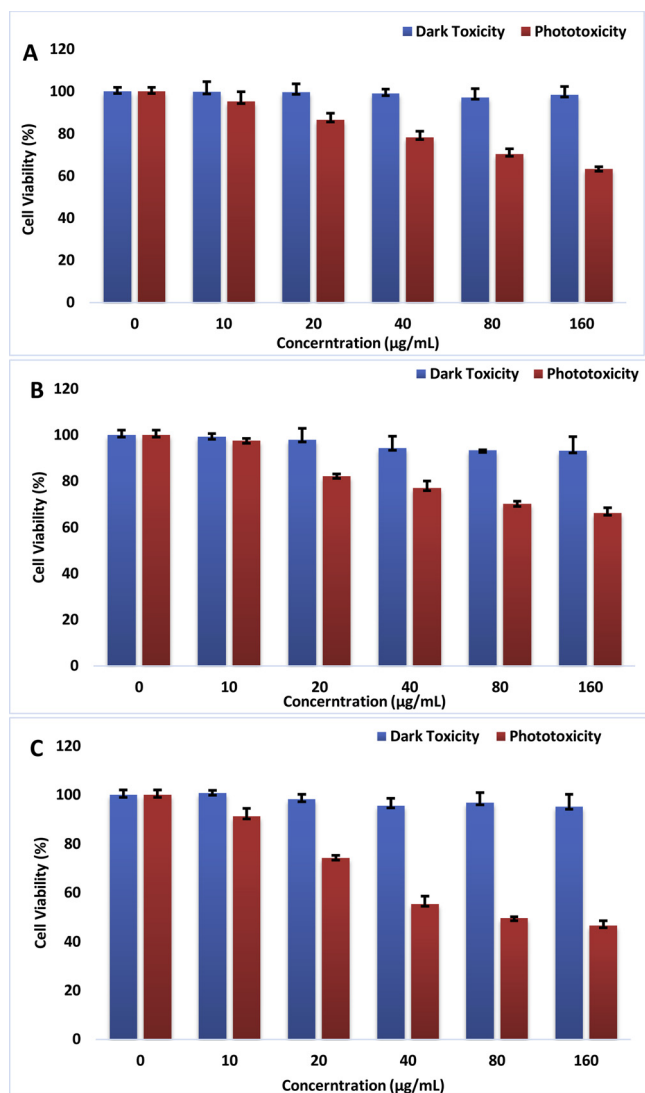toxicity of the photosensitizer is determined by a number of factors including cell type, cellular uptake and localization [48]. The poor solubility and lack of cell targeting moieties in complex **2** could have resulted in poor uptake and localisation of the MPc hence high cell viability.

Complex **2** was linked to GSS nanoparticles as nanocarriers and for improved photophysical properties (through the heavy atom effect of gold), hence the phototoxicity of GSS alone was tested against the MCF–7 cell lines. The highest concentration of GSS (160 μg/mL) showed cell viability of 63% (Fig. 10B), which surprisingly is slightly higher than that of the MPc. Metal nanoparticles are capable of converting certain wavelengths of light into heat. Since GSS alone did not show toxicity in the dark, phototoxicity could probably be due to its photothermal activity as reported before [22]. The conjugate, **2**-GSS afforded improved PDT activity with cell viability of 49% at 80 μg/mL and 46% at 160 μg/mL, Fig. 10C. The enhanced PDT activity for **2**–GSS compared to complex **2** is attributed to enhanced singlet oxygen quantum yield due to the presence of Au, a heavy atom as explained before, in addition to the phototoxicity from GSS.

4. Conclusion

2(3),9(10),16(17),23(24) Tetrakis[(benzo[*d*]thiazol-2-yl phenoxy) phthalocyaninato] zinc(II) (**1**) and 2(3),9(10),16(17),23(24) tetrakis [(benzo[*d*]thiazol-2-yl phenoxy)phthalocyaninato] indium(III) chloride (**2**) were linked to gold speckled silica (GSS) nanoparticles through S-Au/N-Au self-assembly. The conjugates displayed higher triplet and

Fig. 10. Dark toxicity and phototoxicity effects of complex **2** (A), GSS (B) and **2**-GSS (C) against epithelial breast cancer cells (MCF–7). Fixed irradiation dose = 170 J/cm². Control = 1% DMSO in culture media.

singlet oxygen quantum yields compared to their respective Pcs alone. The *in vitro* dark cytotoxicity and phototoxicity of GSS of complex **2** and **2**-GSS against MCF-7 cell line were investigated. They all showed less *in vitro* dark toxicity with ≥ 93% viable cells in all the tested concentrations. **2**-GSS showed enhanced PDT activity compared to **2** alone due to the enhanced singlet oxygen quantum yield and also the phototoxicity of GSS. **2**-GSS has potential for application as a PS in PDT for cancer treatment.

Acknowledgements

Appendix A. Supplementary data

Supplementary material related to this article can be found, in the online version, at doi:https://doi.org/10.1016/j.pdpdt.2019.01.019.

References

[1] G. de la Torre, C.G. Claessens, T. Torres, Phthalocyanines: old dyes, new materials. Putting color in nanotechnology, Chem. Commun. 20 (2007) 2000–2015.
[2] T. Fukuda, N. Kobayashi, UV-visible absorption spectroscopic properties of phthalocyanines and related macrocycles, in: K.M. Kadish, K.M. Smith, R. Guilard (Eds.), Handbook of Porphyrin Science, vol. 9, World Scientific Press, 2010, pp. 1–644.
[3] C.G. Claessens, U.H. Tomas Torres, Phthalocyanines: from outstanding electronic properties to emerging applications, Chem. Rec. 8 (2008) 75–97.
[4] M. Neagu, C. Constantin, M. Tampa, C. Matei, A. Lupu, E. Manole, R.M. Ion, C. Fenga, A.M. Tsatsakis, Toxicologicaland efficacy assessment of post-transition metal (Indium) phthalocyanine for photodynamic therapy in neuroblastoma, Oncotarget 7 (2016) 69718–69732.
[5] D.O. Oluwole, S.L. Manoto, R. Malabi, C. Maphanga, S. Ombinda-Lemboumba, P. Mthunzi-Kufa, T. Nyokong, Evaluation of the photophysicochemical properties and photodynamic therapy activity of nanoconjugates of zinc phthalocyanine linked to glutathione capped Au and Au₃Ag₁ nanoparticles, Dye Pigment. 150 (2018) 139–150.
[6] E. Dube, D.O. Oluwole, E. Prinsloo, T. Nyokong, Gold–chitosan composite with low symmetry zinc phthalocyanine for enhanced singlet oxygen generation and improved photodynamic therapy activity, New J. Chem. 42 (2018) 10214–10225.
[7] M. Tampa, C. Matei, S. Popescu, S.R. Georgescu, M. Neagu, C. Constantin, R.M. Ion, Zinc trisulphonated phthalocyanine used in photodynamic therapy of dysplastic oral keratinocytes, Rev Chimie. 64 (2013) 639–645.
[8] R. Cubbedu, G. Canti, C. D'Andrea, A. Pifferi, P. Taroni, A.J. Toricelli, Effects of photodynamic therapy on the absorption properties of disulphonated aluminum phthalocyanine in tumor-bearing mice, J. Photochem. Photobiol. B. 60 (2001) 73–78.
[9] K. Maduray, B. Odhav, The in vitro photodynamic effect of laser activated gallium, indium and iron phthalocyanine chlorides on human lung adenocarcinoma cells, J. Photochem. Photobiol. B 128 (2013) 58–63.
[10] T. Nyokong, Desired properties of new phthalocyanines for photodynamic therapy, Pure Appl. Chem. 83 (2011) 1763–1779.
[11] K.N. Solov'ev, E.A. Borisevich, Intramolecular heavy-atom effect in the photophysics of organic molecules, Phys. Usp. 48 (2005) 231–253.
[12] K. Hayashi, M. Nakamura, H. Miki, S. Ozaki, Photostable iodinated silica/porphyrin hybrid nanoparticles with heavy-atom effect for wide-field photodynamic/photothermal therapy using single light source, Adv. Funct. Mater. 24 (2014) 503–513.
[13] A. Gorman, J. Killoran, C. O'Shea, T. Kenna, W.M. Gallagher, D.F. O'Shea, *In vitro* demonstration of the heavy-atom effect for photodynamic therapy, J. Am. Chem. Soc. 126 (2004) 10619–10631.
[14] G.M.F. Calixto, J. Bernegossi, L.M.F. Fontana, M. Chorilli, Nanotechnology-based drug delivery systems for photodynamic therapy of cancer: a review, Molecules 21 (2016) 342 (18 pages).
[15] M.E. Wieder, D.C. Hone, M.J. Cook, M.M. Handsley, J. Gavrilovic, D.A. Russell, Intracellular photodynamic therapy with photosensitizer-nanoparticle conjugates: cancer therapy using a 'Trojan horse', Photochem. Photobiol. Sci. 5 (2006) 727–734.
[16] I. Roy, T.Y. Ohulchanskyy, H.E. Pudavar, E.J. Bergey, A.R. Oseroff, J. Morgan, T.J. Dougherty, P.N. Prasad, Ceramic-based nanoparticles entrapping water-insoluble photosensitizing anticancer drugs: a novel drug-carrier system for photodynamic therapy, J. Am. Chem. Soc. 125 (2003) 7860–7865.
[17] I.I. Slowing, J.L. Vivero-Escoto, B.G. Trewyn, V.S.Y. Lin, Mesoporous silica nanoparticles: structural design and applications, J. Mater. Chem. 20 (2010) 7924–7937.
[18] Y. Hoshikawa, H. Yabe, A. Nomura, T. Yamaki, A. Shimojima, T. Okubo, Mesoporous silica nanoparticles with remarkable stability and dispersibility for antireflective coatings, Chem. Mater. 22 (2010) 12–14.
[19] F.K. Alanazi, A.A. Radwan, I.A. Alsarra, Biopharmaceutical applications of nanogold, J. Saudi Pharm. Soc. 18 (2010) 179–193.
[20] C. Kim, P. Ghosh, V.M. Rotello, Multimodal drug delivery using gold nanoparticles, Nanoscale 1 (2009) 61–67.
[21] S. Link, C. Burda, B. Nikoobakht, M.A. El-Sayed, Laser-induced shape changes of colloidal gold nanorods using femtosecond and nanosecond laser pulses, J. Phys. Chem. B 104 (2000) 6152–6163.
[22] J. Chen, B. Wiley, Z.Y. Li, D. Campbell, F. Saeki, H. Cang, L. Au, J. Lee, X. Li, Y. Xia, Gold nanocages: engineering their structure for biomedical applications, Adv. Mater. 17 (2005) 2255–2261.
[23] B. Cheng, H. He, T. Huang, S.S. Berr, J. He, D. Fan, J. Zhang, P. Xu, Gold nanosphere gated mesoporous silica nanoparticle responsive to near-infrared light and redox potential as a theranostic platform for Cancer therapy, J. Biomed. Nanotechnol. 12 (2016) 435–449.
[24] P. Sharma, S.C. Brown, A. Singh, N. Iwakuma, G. Pyrgiotakis, V. Krishna, J.A. Knapik, K. Barr, B.M. Moudgil, S.R. Grobmyer, Near-infrared absorbing and luminescent gold speckled silica nanoparticles for photothermal therapy, J. Mater. Chem. 20 (2010) 5182–5185.
[25] E. Dube, D.O. Oluwole, T. Nyokong, Improved photophysical and photochemical properties of thiopheneethoxy substituted metallophthalocyanines on immobilization with gold–speckled silica nanoparticles, Photochem. Photobiol. 94 (2018) 521–531.
[26] E.E. Gurdal, E. Buclulgan, I. Durmaz, R. Cetin-Atalay, M. Yarim, Synthesis and anticancer activity evaluation of some benzothiazole-piperazine derivatives, Anticancer Agents med, Chem. 15 (2015) 382–389.
[27] N. Nwaji, B. Jones, J. Mack, D.O. Oluwole, T. Nyokong, Nonlinear optical dynamics of benzothiazole derivatized phthalocyanines in solution, thin films and when conjugated to nanoparticles, J. Photochem. Photobio. A Chem. 346 (2017) 46–59.

[28] M. Ambroz, A. Beeby, A.J. McRobert, M.S.C. Simpson, R.K. Svensen, D. Phillips, Preparative, analytical and fluorescence spectroscopic studies of sulphonated aluminium phthalocyanine photosensitizers, J. Photochem. Photobiol. B, Biol. 1 (1999) 87–95.

[29] A. Aktaş, M. Durmuş, L. Değrmencioğlu, Self-assembling novel phthalocyanines containing a rigid benzothiazole skeleton with a 1,4-benzene linker: synthesis, spectroscopic and spectral properties, and photochemical/photophysical affinity, Polyhedron 48 (2012) 80–91.

[30] J. Mack, M.J. Stillman, K.M. Kadish, K.M. Smith, R. Guilard (Eds.), The Porphyrin Handbook, Academic Press, New York, 2003.

[31] E. Gurel, M. Pişkin, S. Altun, Z. Odabaş, M. Durmuş, Synthesis, characterization and investigation of the photophysical and photochemical properties of highly soluble novel metal-free, zinc(II), and indium(III) phthalocyanines substituted with 2,3,6-trimethylphenoxy moiety, Dalton Trans. 44 (2015) 6202–6211.

[32] K. Sakamoto, E. Ohno-Okumura, T. Kato, H. Soga, Synthesis of near-infrared absorbed metal phthalocyanine with S-aryl groups at non-peripheral positions, J. Porphyrins Phthalocyanines 14 (2010) 47–54.

[33] M.J. Stillman, T. Nyokong, Leznoff CC (Ed.), Lever ABP Phthalocyanines: Properties and Applications, vol. 1, VCH Publishers, New York, 1989Ch 3, p. 133.

[34] L. Li, J.F. Zhao, N. Won, H. Jin, S. Kim, J.Y. Chen, Quantum dot - aluminum phthalocyanine conjugates perform photodynamic reactions to kill cancer cells via fluorescence resonance energy transfer (FRET), Nanoscale Res. Lett. 7 (2012) 386–393.

[35] R. Prabakaran, R. Kesavamoorthy, G.L.N. Reddy, F.P. Xavier, Structural Investigation of copper phthalocyanine thin films using X-Ray diffraction, Raman scattering and optical absorption measurements, Phys. Status Solidi 229 (2002) 1175–1186.

[36] M.H. Majles Ara, Z. Dehghani, R. Sahraei, A. Daneshfar, Z. Javadi, F. Divsar, Diffraction patterns and nonlinear optical properties of gold nanoparticles, J Quant Spectrosc. Radiat. Transfer 113 (2012) 366–372.

[37] R. Jenkins, R.L. Synder, Introduction to X-ray Diffractometry, Wiley and Sons, New York, 1996.

[38] J.W. Owens, M.J. Robins, Phthalocyanine photophysics and photosensitizer efficiency on human embryonic lung fibroblasts, J. Porphyrins Phthalocyanines 5 (2001) 460–464.

[39] Z. Petrásek, D. Phillips, A time-resolved study of concentration quenching of disulfonated aluminium phthalocyanine fluorescence, Photochem. Photobiol. Sci. 2 (2003) 236–244.

[40] Z.N. Erol, P. Atienzar, Y. Arslanoğlu, E. Hamuryudan, H. García, Synthesis and photophysical properties of phthalocyanines having calixpyrrole units, RSC Adv. 5 (2015) 55901–55908.

[41] M.G. Debacker, O. Deleplanque, B. Van Vlierberge, F.X. Sauvage, A laser photolysis study of triplet lifetimes and of triplet–triplet annihilation reactions of phthalocyanines in DMSO solutions, Laser Chem. 8 (1988) 1–11.

[42] J.R. Darwent, P. Douglas, A. Harriman, G. Porter, M.C. Richoux, Metal phthalocyanines and porphyrins as photosensitizers for reduction of water to hydrogen, Coord. Chem. Rev. 44 (1982) 83–126.

[43] R.R. Allison, K. Moghissi, Oncologic photodynamic therapy: clinical strategies that modulate mechanisms of action, Photodiagnosis Photodyn. Ther. 10 (2013) 331–341.

[44] M.C. DeRosa, R.J. Crutchley, Photosensitized singlet oxygen and its applications, Coord. Chem. Rev. 233/234 (2002) 351/371.

[45] A. Ogunsipe, J. Chen, T. Nyokong, Photophysical and photochemical studies of zinc (II) phthalocyanine derivatives—effects of substituents and solvents, New J. Chem. 28 (2004) 822–827.

[46] J.L. Sessler, W.C. Dow, D.O. Connor, A. Harriman, G. Hemmi, T.D. Mody, R.A. Miller, F. Qing, S. Springs, K. Woodburn, S.W. Young, Biomedical applications of lanthanide (III) texaphyrins Lutetium(III) texaphyrins, J. Alloys. Compd. 249 (1997) 146–152.

[47] D.O. Oluwole, E. Prinsloo, T. Nyokong, Photophysicochemical properties of nanoconjugates of zinc(II) 2(3)-mono-2-(4-oxy)phenoxy)acetic acid phthalocyanine with cysteamine capped silver and silver–gold nanoparticles, Polyhedron 119 (2016) 434–444.

[48] D. Atilla, N. Saydan, M. Durmus, A.G. Gurek, T. Khan, A. Ruck, H. Walt, T. Nyokong, V. Ahsen, Synthesis and photodynamic potential of tetra-and octa-triethyleneoxysulfonyl substituted zinc phthalocyanines, J. Photochem. Photobiol. A: Chem. 186 (2007) 298–307.